Aggregation behavior of polystyrene-b-poly(acrylic acid) at the air–water interface

ARTICLE *in* SOFT MATTER · DECEMBER 2012

Impact Factor: 4.03 · DOI: 10.1039/C2SM26797G

3 AUTHORS, INCLUDING:

Xiaolu Wang
Université de Montpellier
3 PUBLICATIONS **23** CITATIONS
SEE PROFILE

D. Y. Zang
Northwestern Polytechnical University
32 PUBLICATIONS **236** CITATIONS
SEE PROFILE

Soft Matter

RSC Publishing

PAPER

View Article Online
View Journal | View Issue

Cite this: *Soft Matter*, 2013, 9, 443

Aggregation behavior of polystyrene-*b*-poly(acrylic acid) at the air–water interface†

Xiaolu Wang,[ab] Xiaoyan Ma*[ab] and Duyang Zang[a]

The aggregation behavior of amphiphilic block copolymer polystyrene-*b*-poly(acrylic acid) (PS-*b*-PAA) at the air–water interface was investigated through surface pressure measurements (isotherms, compression–expansion hysteresis and compression relaxation experiments), Brewster Angle Microscopy (BAM) imaging and Atomic Force Microscopy (AFM) imaging. It is found that PS-*b*-PAA (M_n = 11 490 g mol^{-1}, PAA wt%~62%) forms a stable Langmuir monolayer on the water surface (pH = 7) by using *N*,*N*-dimethylformamide (DMF) as the spreading solvent. The aggregation of block copolymer is induced by an initial diffusion of DMF into water from the interface. Upon compression of the film, the pseudoplateau observed in the Langmuir isotherm corresponds to a "pancake-to-brush" transition with the PAA chains gradually dissolving in the water subphase and stretching underneath the PS cores. Based on the isotherms and the BAM images, it is suggested that the polymer chain dynamics in spreading solutions with different concentrations at the time of solvent diffusion influence the interfacial behavior of block copolymers significantly. The Langmuir–Blodgett (LB) films prepared at different surface pressures from different spreading solution concentrations were scanned by AFM. A variety of morphologies such as wormlike, porous and reticulate structures, and dots were observed. The isotherms and AFM images show the spreading solution concentration and surface pressure dependence of the aggregation behavior of PS-*b*-PAA copolymer at the air–water interface.

Received 2nd August 2012
Accepted 10th October 2012

DOI: 10.1039/c2sm26797g

www.rsc.org/softmatter

Introduction

Block copolymers are quite essential nanostructure forming materials thanks to their self-organizing capabilities due to the combination of polymer blocks containing different, unique properties. Taking advantage of the different ordered morphologies produced, a large variety of potential technological applications including information storage, drug delivery, and photonic crystals are feasible. As a kind of special block copolymer, amphiphilic diblock copolymer containing separate hydrophobic and hydrophilic portions has increased surface activity and it can stay adsorbed at the air–water interface beyond the collapse pressure of the individual blocks. Many amphiphilic block copolymers have been exploited to control interfacial properties at the air–water interface,[1] where a hydrophobic block anchors the hydrophilic soluble block to the free surface, and they can form stable films and aggregate into a variety of morphologies. As an effective method to prepare ultrathin films, the Langmuir–Blodgett (LB) technique can be utilized, and the Langmuir isotherms and AFM images are also frequently used to reveal the surface pressure and aggregates morphology changes upon compression of the films. Most of the investigations are focused on poly(ethylene oxide) (PEO) based block copolymers, especially the copolymers with PEO and polystyrene (PS) blocks with structures such as linear,[2–9] star-shaped[10–15] and hyperbranched.[16] Moffitt's team[3–9] found that PS-*b*-PEO copolymer could form a stable monolayer on the water surface and the typical Langmuir isotherm contained three regions, an initial region corresponding to the PEO adsorbed in a two dimensional (2D) "pancake" structure, a pseudoplateau region corresponding to adsorbed PEO segments desorbed from the interface and immersed in the water subphase, and a "brush" region with a sharp increase in surface pressure corresponding to the PEO chains stretched into water from the underneath of PS cores. The air–water interfacial behavior of some other amphiphilic block copolymers such as pH-responsive polystyrene-*b*-poly(vinyl pyridine),[17,18] charged poly(hydrogenated isoprene)-*b*-poly(styrenesulfonate)[19] and some acrylate based polymers such as poly(1,1-diethylsilacyclobutane)-*b*-poly(methacrylic acid),[20] poly(isoprene)-*b*-poly(acrylic acid),[21] and poly(hydrogenated isoprene)-*b*-poly(acrylic acid)[22] has also been studied.

[a]*Key Laboratory of Space Applied Physics and Chemistry, Ministry of Education, Shaanxi Province, School of Science, Northwestern Polytechnical University, Xi' an 710072, China. E-mail: m_xiao_yana@nwpu.edu.cn; Fax: +86-29-88491826; Tel: +86-29-88431676*

[b]*Key Laboratory of Polymer Science and Technology, Shaanxi Province, School of Science, Northwestern Polytechnical University, Xi' an 710072, China*

† Electronic supplementary information (ESI) available: Polymer synthesis details, characterization data (GPC chromatograms, FT IR and NMR spectra) and compression isotherms of the PS-*b*-PAA copolymer at the air–water interface, obtained from spreading concentrations 3 mg mL^{-1} and 18 mg mL^{-1}. See DOI: 10.1039/c2sm26797g

As weak polyacids, PAA ($pK_a \approx 5.5$) based copolymers show interesting interfacial behaviors. The ionization degree of carboxylic acid groups in water is strongly pH-dependent. In the research on rheology and phase behavior of P_nBA_{100}-*b*-PAA_{150} in aqueous solutions, Eghbali *et al.*[23] found that when the degree of neutralization was over 0.1 the solution did not exhibit any surface activity. Charged PAA chains are hydrophilic and thus nonsurface active. Meanwhile, the physical and chemical properties of the other block in these diblock copolymers with PAA, as well as the block ratio, have a significant influence on their behavior at the air–water interface. For the PS-*b*-PAA copolymer, many research studies have been performed.[24–29] The earliest study on the surface monolayer of PS-*b*-PAA was reported by Baskir *et al.*[24] in 1988. The properties of PS-*b*-PAA block copolymer monolayers have been studied using Langmuir isotherms as a function of subphase pH value in previous literature. Currie *et al.*[27] investigated surface pressure isotherms of linear PS_{33}-*b*-PAA_{368} at pH 4.7. For PS-*b*-PAA dendrimer-like block copolymer with 93 wt% PAA (M_n = 129 000 g mol^{-1}), Joncheray *et al.*[28] carried out isotherms of Langmuir films under acid conditions (pH = 2.5). In their work, typical isotherms similar to those of PEO diblock copolymers were observed, and the pseudoplateaus were supposed to correspond to a pancake-to-brush transition with the PAA chains dissolving in the water subphase. However, the copolymers used both have longer PAA chains. It was found that under the condition of pH > 6, PAA blocks deprotonated. Meanwhile the PS wt% in copolymers was too low to allow it to act as an anchor, and as a result no stable monolayer could be formed at the air–water interface. For PS-*b*-PAA with longer PS chains investigated by Niwa *et al.*[25] and Muller *et al.*,[29] stable monolayers were prepared on pure water, but no pseudoplateaus could be seen in the isotherms. Therefore, the ratio of hydrophobic block in copolymer and water subphase pH value both play important roles in the behavior of block copolymers at the air–water interface.

With regard to the formation of block copolymer aggregates at the air–water interface, there exist many different views. Cox *et al.*[30] summarized the three main opinions: (1) transfer of micelles in the spreading solution to the surface; (2) compression induced surface aggregation; and (3) spontaneous surface aggregation along with removal of solvent. Their research on PS-*b*-PEO supported the third view and they found that after the removal of solvent the block copolymer formed micelles instead of separate spreading on the water surface. In 2009, Moffitt's team[9] reported an interesting phenomenon that at the air–water interface PS homopolymer could self-assemble into aggregates with different structures such as strand, network and continent *via* the removal of spreading solvent. Meanwhile, there are also many other research studies[5,10,17,30–32] which have demonstrated the formation of monolayers with block copolymer aggregates on the water surface.

Cheyne and Moffitt[5] also found that the formation of amphiphilic diblock copolymer surface aggregates was the result of spontaneous copolymer aggregation starting with an initial dewetting of the copolymer spreading solution caused by the evaporation of solvent from the water surface. It could be deduced that the solvent used to prepare the copolymer spreading solution may also influence the air–water interfacial self-assembly behavior of PS-*b*-PAA. PAA does not dissolve in common organic spreading solvents (chloroform, toluene, *etc.*) because of its polarity. Mixtures of solvents such as dioxane–toluene mixture[27] and ethanol–chloroform[28] were used to prepare PS-*b*-PAA copolymer spreading solution. It is difficult to analyze the detailed mechanism of the formation of copolymer aggregates since evaporation and dissolution of the mixed solvents occur simultaneously at the point of spreading the copolymer solution onto the water surface. Drawing inspiration from the self-assembly of PS-*b*-PAA in solution induced by dialyzing against water, we chose DMF as the co-solvent of PS-*b*-PAA. As DMF is water soluble and less volatile and its density is lower than that of water, when the solution of PS-*b*-PAA is spread on water, DMF not only spreads on the water surface, but also exchanges with the water underneath which is similar to dialysis. Induced by this, micelles of PS-*b*-PAA at the air–water interface were supposed to be formed initially.

In the present paper, we study the aggregation behavior of PS-*b*-PAA at the pure water surface by using DMF as the spreading solvent. The surface pressure–mean molecular area isotherms, Brewster Angle Microscopy (BAM) images of Langmuir films, and the AFM images of LB films are explored. Especially the compression elastic modulus of the PS-*b*-PAA Langmuir film is obtained through compression–relaxation analysis. Meanwhile, we also investigate the effect of spreading solution concentration and surface pressure on the interfacial formation of PS-*b*-PAA aggregates. On the basis of these testing results, mechanisms of the formation of two dimensional aggregates are discussed.

Experimental section

Materials

The PS-*b*-PAA block copolymer used in this study was synthesized through reversible addition–fragmentation chain transfer (RAFT) polymerization. The PS macro-initiator was first synthesized in bulk by RAFT polymerization using benzyl dithiobenzoate as the chain transfer agent.[33,34] The number average molecular weight (M_n) measured by gel permeation chromatography (GPC) was about 4368 g mol^{-1} and the M_w/M_n (PDI) was about 1.23. PS-*b*-PAA was synthesized by RAFT polymerization using AIBN as initiator and PS as macro-initiator. The M_n was about 11 490 g mol^{-1} and the PDI was about 1.35 as listed in Table 1 (x_n indicates the degree of polymerization of each block). The polymers were also analyzed *via* FT IR and ^{1}H NMR as shown in Fig. S3 and S4 in ESI.†

The stock solutions of various spreading concentrations were prepared by weighing an appropriate amount of the polymer (dried overnight in a dark vacuum drying oven at room

Table 1 GPC analysis results of PS-*b*-PAA

	M_n (g mol^{-1})	M_w (g mol^{-1})	M_w/M_n	$M_{n,PAA}$	$M_{n,PS}$	$x_{n,PAA}$	$x_{n,PS}$	PAA (wt%)
PS-*b*-PAA	11 490	15 590	1.35	7122	4368	99	42	62

temperature prior to use) into new glass reagent vials cleaned three times with acetone in an ultrasonic cleaning tank, and then a certain amount of distilled DMF was added gravimetrically; all solutions were prepared 24 h prior to use to allow for equilibration and used within 1 day for isotherm trials.

Isotherms of Langmuir films and BAM imaging

Surface pressure measurements were accomplished using the Langmuir trough system ($W = 200$ mm, $L = 310$ mm, JML04C3, Powereach Ltd., China) equipped with two moving barriers and a Wilhelmy plate. Prior to use, the trough was first cleaned with abstergent and dipped in $NaCO_3$ solution, after being rinsed several times with ultra-pure water, CH_2Cl_2 was used to scrub the trough to make it cleaner and much more hydrophobic. Meanwhile, the roughened platinum Wilhelmy plate was dipped in HNO_3 for 1 h and rinsed with ultra-pure water several times.

The block copolymer used has a relatively smaller molecular weight, and acrylic acid groups in PAA partly ionize in neutral water leading to small cross-sectional molecular area, so we tend to use more block copolymer. Meanwhile, DMF is soluble in water; thus, it should be used in a suitable amount to avoid possible influence on the water subphase. Furthermore, lower polymer chain dynamics on the water surface lead to easier formation of polymer aggregates. Therefore a higher spreading solution concentration is preferred. In the present paper, a range of spreading solution volumes corresponding to different concentrations (3, 5, 6, 9, 12, 18 mg mL^{-1}) were used to maintain a constant mass (1.5 mg) of deposited copolymer. To prepare a Langmuir film, the PS-*b*-PAA solution in DMF was spread dropwise on an ultra-pure water subphase of neutral pH value using a microsyringe, and the solvent was allowed to dissolve in water for 3 h. The dissolution of DMF contributes to the risk of contaminating the water subphase which may lead to change of surface pressure. In order to test this possibility, 500 μL of pure DMF was deposited onto the water surface and then allowed to dissolve in water for 3 h to examine its compression isotherm, and no significant changes in surface pressure could be observed, indicating that up to this volume the use of the water-soluble and less volatile solvent DMF does not affect the isotherms of the copolymer Langmuir film.

The Langmuir trough was also equipped with a Brewster Angle Microscope (JB04, Powereach Ltd., China) to image the copolymer and its solution films at the interface.

In all experiments, the subphase temperature was 20 ± 2 °C and two hydrophobic barriers compressed the spread film symmetrically and bilaterally at a rate of 3 mm min^{-1}. Isochoric experiments yielded plots of surface pressure *versus* time. Isotherms and compression–expansion hysteresis experiments on the monolayers yielded plots of surface pressure (π) *versus* surface area. The corresponding surface pressure (π) *versus* mean molecular area (MMA) isotherms were obtained by using the calculation method first used by Irving Langmuir in 1917.[35]

Langmuir–Blodgett films

A series of LB films were prepared through depositing corresponding Langmuir films from copolymer solutions of different concentrations at different surface pressures onto new glass substrates. The glass substrates were cleaned by abstergent and ultra-pure water and sonicated in acetone, and dried in a vacuum drying oven. Then they were immersed in the water subphase before spreading copolymer solution. Following maintenance at the desired transfer pressure for 10 min, the submerged substrate was lifted vertically through the film at a rate of 0.5 mm min^{-1}. These transferred films were dried in a vacuum desiccator for 24 h at room temperature and used within a week.

Atomic force microscopy

All the LB films were scanned in the tapping mode with AFM (MFP-3D-SA, Asylum Research Inc., USA) using silicon probes (AMCL-AC240, Olympus, Japan). Each sample was imaged several times at different locations on the substrate to ensure reproducibility. In all cases, the imaging of LB films was performed far from the edge of the glass substrate to minimize any local effects caused by turbulent water flow at the boundary and meniscus effects during transfer.

Results and discussion

BAM images

As shown in Fig. 1, BAM imaging was used to observe the aggregation of block copolymer solution on the water surface before compression. The compressed copolymer films during the expansion process have also been observed. These could

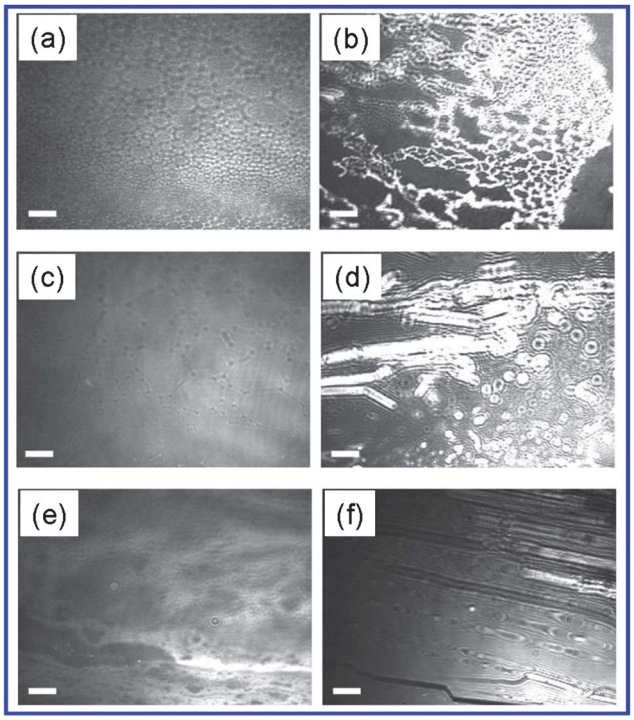

Fig. 1 BAM images of PS-*b*-PAA solution films observed during the process of DMF dissolution (a, c, and e) and copolymer (b, d, and f) films observed following the expansion process, and the spreading solution concentrations are 6 mg mL^{-1} (a and b), 9 mg mL^{-1} (c and d), and 12 mg mL^{-1} (e and f). The bars in all the images are 200 μm.

give us a brief description of how the copolymer solution spreads and how the copolymer aggregates at the water surface when using DMF as the spreading solvent. The discrepancies in the conformation of films can clearly be observed when the spreading solution concentrations are different.

As shown in Fig. 1a, it's found that under a spreading concentration of 6 mg mL^{-1}, the film formed from copolymer solution at the air–water interface shows a continuous network structure with circular meshes. This is very similar to the film of pure solvent spreading at the interface. In the continuous expansion stage after compression, the copolymer aggregates become reticulate structures with irregular meshes as shown in Fig. 1b. However, the reticulate structure is not continuous and some of the meshes are open because of the film collapse along with expansion. During the dissolution of DMF, the copolymer solution film obtained from 9 mg mL^{-1} (Fig. 1c) is slightly different from that obtained from 6 mg mL^{-1}. The morphology is a continuous network, but the meshes are irregular polygons and in their vertexes apparent copolymer solution aggregates can be seen. In the expansion region, the morphologies are rodlike and dot structures (Fig. 1d). The rodlike structures may come from the wrinkles of the film formed upon compression which were separated from each other following film expansion. As exhibited in Fig. 1e, the film of 12 mg mL^{-1} copolymer solution is porous and is very different from that of 6 mg mL^{-1} and 9 mg mL^{-1}. It is attributed to the high concentration causing restriction of polymer chain dynamics. Fig. 1f shows that the film of copolymer observed after expansion is a continent-like structure with rodlike conformations and wrinkles on it, and it is relatively dense. The various behaviors of films from spreading solutions with different concentrations are because of the different polymer chain dynamics.[5] Under the condition of a higher concentration, the initial polymer density after deposition is high. This causes the lower fluidity of polymer at the water surface and also less solvent is present. Therefore the self-assembly morphology can be trapped by polymer immobility when the horizontal spreading and vertical diffusion of DMF are far from complete.

It has been reported in previous research studies[5,36,37] that the dewetting of liquid polymer films from the surface is the mechanism of the formation of initial 2D micelles. However, different from those volatile solvents (such as benzene,[27] chloroform[28]) used, the spreading solvent DMF is miscible with water. Therefore the aggregate formation process should have some differences.

According to the above results, the qualitative model of the initial formation of PS-*b*-PAA aggregates after depositing the solution on the water surface is proposed as shown in Fig. 2. The density of DMF is lower than that of water; thus at the moment of deposition the copolymer solution just disperses on the water surface without being brought into water subphase (Fig. 2a). At the interface of water and polymer solution, a diffusion layer is formed by the spreading of water and DMF (Fig. 2b). Driven by the repulsion between PS and water subphase, the PS chains move upward to the DMF layer. Meanwhile PAA chains can dissolve in both DMF and water, and they cannot restrict the movement of PS chains. Along with the dissolution of DMF, the PS chains gradually move upwards and entangle in the water–DMF mixed solvent (Fig. 2c). When DMF fully dissolves in water subphase (Fig. 2d), the hydrophobic PS clusters orient toward the air anchoring polymers at the interface, while PAA chains stretch peripherally and underneath the PS cores.

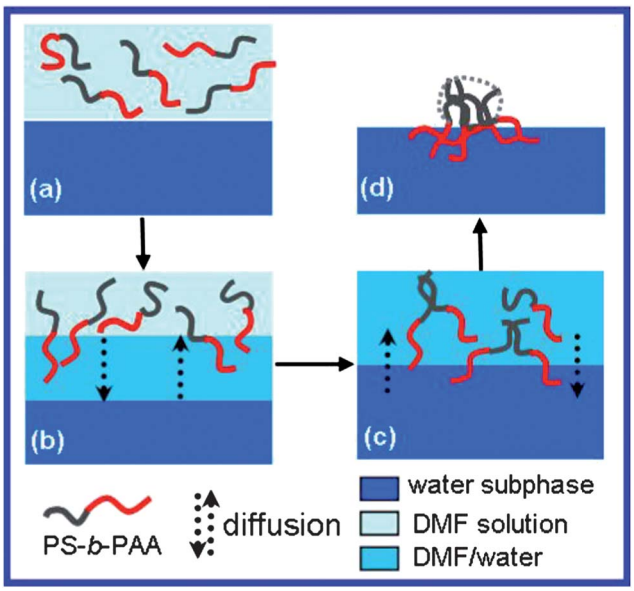

Fig. 2 Initial formation of PS-*b*-PAA aggregates at the air–water interface relative to the time scales of diffusion of DMF. The dotted arrows represent exchange between DMF and water. (a) Initial state after deposition with no diffusion; (b) ideal description of the diffusion of DMF and water at the interface between solution and water subphase; (c) entanglement of PS chains in the mixed solvent; and (d) full dissolution of DMF in water.

Surface pressure–mean molecular area (π–MMA) isotherms

The compression isotherms of Langmuir films obtained from the spreading of PS-*b*-PAA solution with different concentrations on the water surface are shown in Fig. 3a. An apparent spreading concentration (c = 5–12 mg mL^{-1}) dependence of the isothermal film behavior is highlighted. We can also find that all of the isotherms have a low surface pressure at a large mean molecular area (MMA), which suggests the formation of smooth, uniform monolayers. All curves exhibit pseudoplateaus corresponding to a "pancake-to-brush" transition in the intermediate region, followed by a steep increase in surface pressure in the small mean molecular area region.

In Region 1 as exhibited in Fig. 3b, initially the surface film expands at large molecular areas. The neighboring PS chains pack into the core above the interface to avoid unfavorable interactions with water, while PAA chains are anchored at the interface, forming a pancakelike morphology.[28] Because of the ionization and dissolution, PAA chains which radiate from the PS cores are partially soluble in the vicinity of the water subphase and partially adsorbed at the air–water interface. Meanwhile, the neighboring aggregates are not in touch with each other and lateral compression causes only an increase in polymer density on the water surface. The limiting mean

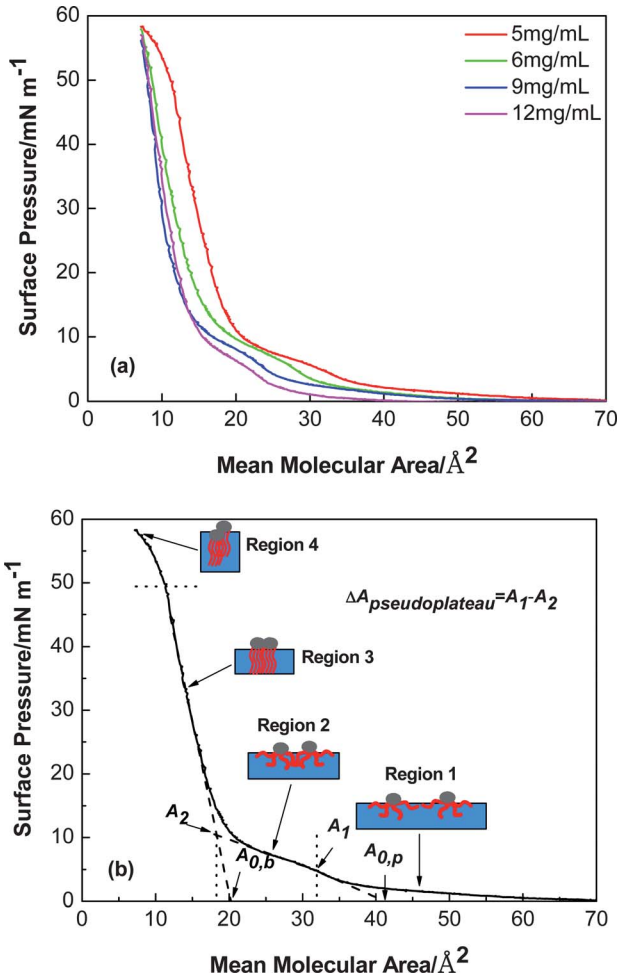

Fig. 3 (a) Compression isotherms of the PS-*b*-PAA copolymer at the air–water interface, obtained from different spreading concentrations (5 mg mL^{-1}, 6 mg mL^{-1}, 9 mg mL^{-1}, 12 mg mL^{-1}). (b) Determination of the brush limiting area $A_{0,b}$, the pancake limiting area $A_{0,p}$ and the width of pseudoplateau $\Delta A_{pseudoplateau}$. Schematic depiction of polymer aggregates in different regions is shown in panel (b).

molecular area of this pancake region could be quantified by extrapolating tangents to the inflection points of the π–MMA curves to a pressure of zero, yielding $A_{0,p}$ (Fig. 3b).

Upon further compression till Region 2 as shown in Fig. 3b, the isotherms exhibit pseudoplateaus corresponding to a "pancake-to-brush" transition which is driven by the lateral compression and interaction among PAA chains. In this region, the overlapping PAA chains gradually dissolve into water and form a quasi brush shape, leaving only the PS clusters anchored atop the surface. The electrostatic and steric repulsions between PAA chains are assumed to be the dominant factors for the formation of the PAA brush. The width of pseudoplateau $\Delta A_{pseudoplateau}$ could be obtained as the distance between two vertical dotted lines shown in Fig. 3b.

After the pseudoplateau is the "brush" region. Due to the interaction of the relatively incompressible PS clusters and the steric repulsion between PAA brushes, the surface pressure rapidly increases and the adjacent copolymer aggregates gradually compress with each other. In this Region 3, extrapolation of the linear portion of the isotherm to the surface pressure of zero yields the limiting mean molecular area of the brush $A_{0,b}$ (Fig. 3b). In Regions 2 and 3, lateral compression of the film results in conformation changes of aggregates; however, the packed PS cores still anchor polymers at the interface preventing them from being transferred to water bulk. At the end of the isotherm, there is a decreasing trend in the increasing rate of surface pressure along with compression, corresponding to Region 4. It is caused by the collapse of the polymer film which is attributed to over-compression of the relatively uncompressible PS aggregates. It should be noticed that in this region PS cores overlapped with each other leading to immersion of some polymer aggregates in water.

For the range of spreading concentrations, the mean molecular areas of the pancake and brush conformations and the width of pseudoplateau ($A_{0,p}$, $A_{0,b}$, and $\Delta A_{pseudoplateau}$ respectively) are shown in Fig. 4. Interestingly, the trend in this figure highlights a spreading concentration dependence of the pancake limiting area. The $A_{0,p}$ decreases with the rise in concentration, up to a relatively constant value (~27 Å^2) for higher spreading concentrations (≥12 mg mL^{-1}). $\Delta A_{pseudoplateau}$ almost linearly decreases with the rise in concentration. However, with the increase of spreading concentration, $A_{0,b}$ firstly decreases for dilute concentrations (≤9 mg mL^{-1}) and then rises for higher spreading concentrations (≥9 mg mL^{-1}).

The changes of $A_{0,p}$, $A_{0,b}$, and $\Delta A_{pseudoplateau}$ *versus* spreading solution concentrations could be explained by the discrepancies of interfacial chain dynamics after spreading. When deposited onto the water surface, the fluidity of spreading solution could be affected greatly by the solution concentration. For a dilute solution, the block copolymer spreads well on the water surface and the polymer chain dynamics are high. The attraction between PAA and water and the steric repulsion between PS and PAA provide a driving force for the system to decrease the density of PS packing within the aggregates. This leads to a loosened PS core above the interface. Meanwhile PAA chains radiate from the PS cores and occupy a relatively larger surface

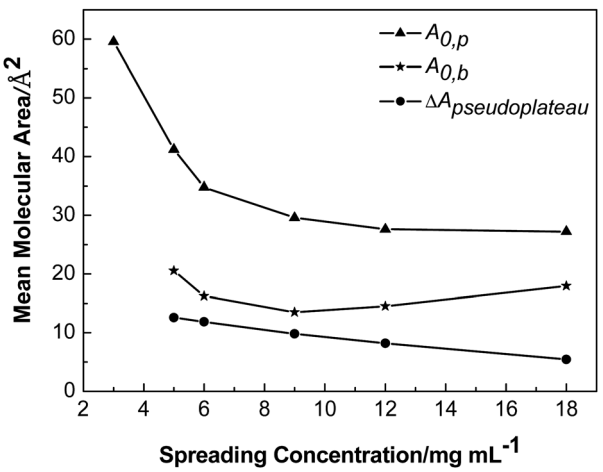

Fig. 4 Plots of pancake limiting area $A_{0,p}$, brush limiting area $A_{0,b}$ and the width of pseudoplateau $\Delta A_{pseudoplateau}$ *versus* spreading concentration of the PS-*b*-PAA copolymer determined from compression isotherms.

area. Thus, the $A_{0,p}$ value is higher for films from a lower concentration solution. When the spreading solution concentration is high, the polymer chain dynamics are low, and therefore dense, less energetically favorable aggregate conformations are trapped by solvent removal and vitrification. Strong repulsive interactions are expected underneath the PS cores, forcing PAA chains in the sublayer to submerge into water even before the aggregates are compressed. Therefore the copolymers occupy a small surface area. Upon compression, the peripheral PAA chains are brought into touch, and the interactive distance (the width of pseudoplateau) is decided by the cross-sectional length of PAA chains absorbed at the interface which is comparable to $A_{0,p}$ value, and hence $\Delta A_{pseudoplateau}$ is higher for dilute solutions. In the brush region, the PAA chains are fully desorbed from the interface, and therefore the limiting mean molecular area is mainly determined by both the size of PS clusters and the uncompressible interspaces between them which are related to the morphologies of copolymer aggregates in the brush region.

Hysteresis and relaxation

Hysteresis has been proved to be very informative in elucidating the dynamic behavior of amphiphilic systems under variable stress at the air–liquid interface. Meanwhile, measuring the stress relaxation as a function of time after a step compression is a very useful method to characterize the viscoelasticity of copolymer films at the interface.

Hysteresis behaviors of films from a 12 mg mL^{-1} copolymer solution in pancake, pancake-to-brush and brush regions were investigated and are shown in Fig. 5. From the first circle in the pancake region we find that there is no apparent hysteresis, which illustrates that the block copolymer aggregate freely diffuses at the interface. The second circle in the pancake region has slight hysteresis after expansion, and the hysteresis could be explained by the hydration of PAA chains during the transition. The first circle in the brush region initially shows a sharp drop in surface pressure upon expansion and then a smooth decrease. This is attributed to the local ordering and cohesion of PAA chains in the brush conformation. The second circle in the brush region shows similar behavior as the first circle, and the slight shift comes from entanglement of the PAA chains during the first circle and a time lag for disentanglement in the following process.

We also studied the relaxation behavior of the polymer film *via* a step compression method. In the case of surface film, it was firstly compressed, and afterwards the barriers were stopped to allow the relaxation of the monolayer. As exhibited in Fig. 6a, the surface pressure increases quickly and then relaxes to an equilibrium value, illustrating that the monolayer is viscoelastic. Note that the relaxation is very slow and it takes a long time to reach equilibrium. The variation of surface pressure *versus* MMA is also shown in the inset in Fig. 6a.

To further study the relaxation mechanisms involved, we use an exponential function to fit the surface pressure curves obtained in step compression experiments. In the simplest case, when there is only one relaxation time, the pressure varies exponentially with time as $e^{-t/\tau}$ (τ is the relaxation time).[38–40] Here we choose single exponential and two exponentials to fit

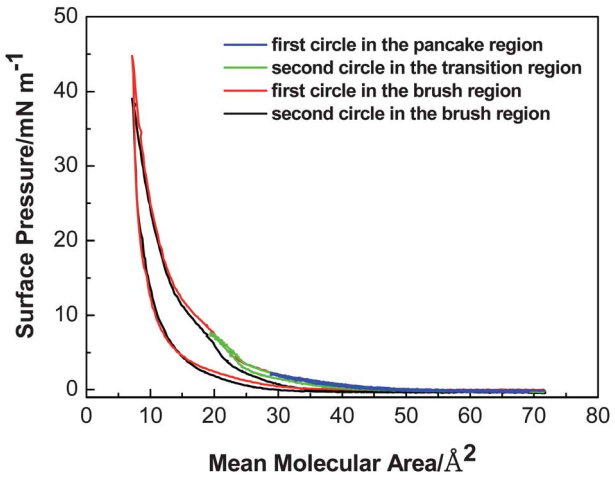

Fig. 5 Compression–expansion cycles of the PS-*b*-PAA copolymer films at high and low surface pressures at the rate of 9.71 mm min^{-1} following spreading from a 12 mg mL^{-1} copolymer solution.

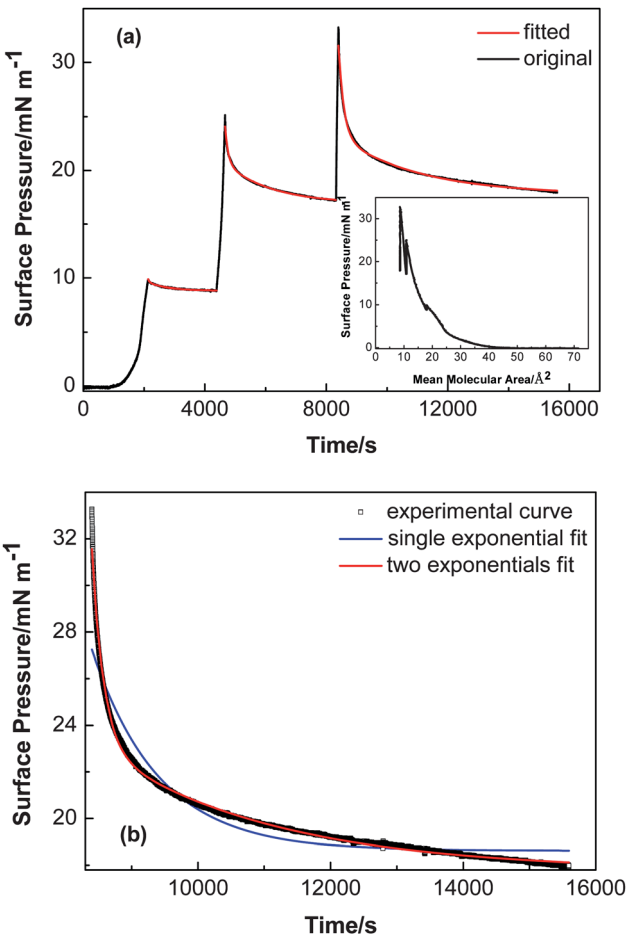

Fig. 6 (a) Surface pressure as a function of time in a step compression experiment from 12 mg mL^{-1} spreading PS-*b*-PAA copolymer solutions and the corresponding exponential fitting curves. The inset corresponds to step compression π–MMA isotherms of (a). (b) Examples of relaxation curve and the corresponding two fitting curves at an MMA of 9 Å^2.

Table 2 Compression modulus and the relaxation times from fits of pressure–time evolution with eqn (2)

MMA (Å^2)	$E(0)$ (mN m^{-1})	τ_1 (s)	τ_2 (s)
18	1.03	49	663
11	7.16	107	1543
9	13.79	175	2640

the relaxation curves. The time variation of the compression modulus can be written as eqn (1) and (2):

$$E(t) = E_0 e^{-t/\tau} \quad (1)$$

$$E(t) = E_1 e^{-t/\tau_1} + E_2 e^{-t/\tau_2} \quad (2)$$

where E is the compression modulus, and E_0, E_1 and E_2 are the moduli corresponding to different relaxation times τ, τ_1 and τ_2 respectively.

As shown in Fig. 6a and b, we found that the two exponential fitting curves fit the original relaxation curves better than the single exponential one. The main interest of the fits is to obtain the modulus and relaxation time of the copolymer films. The modulus at short time can be obtained as $E(0) = E_1 + E_2$, and the value of the compression elastic modulus and the relaxation times deduced from fits of pressure–time evolution with eqn (2) are listed in Table 2.

As can be observed in Table 2, the times necessary for surface pressures to reach constant values are all quite long in different regimes and the compression modulus and relaxation times all increase with the decrease of the mean molecular area (MMA). The good fit of curves using eqn (2) suggests that there are at least two physical mechanisms that dominate the relaxation process. The non-equilibrium effect caused by the fast compression can relax through[41,42] (1) damping of surface fluctuation and (2) motion of polymer aggregates inside the films. τ_1 are all in the time scale of <180 s, and this may represent the damping dynamics of films caused by surface fluctuation from the stop of barriers. τ_2 is much longer than τ_1, and it reflects the arrangement of polymer aggregates inside the films which results in the conformation changes. This can also be demonstrated by the following AFM results.

Surface morphologies of Langmuir–Blodgett films

To highlight the spreading and surface pressure dependence of aggregate morphologies, films from various spreading concentrations were transferred to glass substrates at different surface pressures and scanned by the AFM. Previous literature[43] reported that the morphology of amphiphilic organic materials in their monolayer state is usually preserved during the transfer under the optimal transfer conditions. Representative AFM images are shown in Fig. 7–9. The compression speed and the rate of lifting of glass substrates were kept constant at 3 mm min^{-1} and 0.5 mm min^{-1}, respectively. These parameters were shown to have a minimal influence on the overall aggregate structure. In all images the light regions represent the raised PS cores of the aggregates.

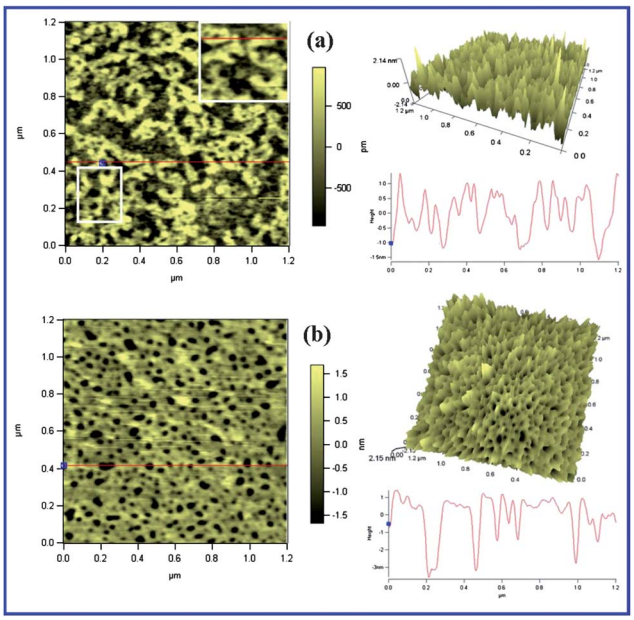

Fig. 7 Topography and 3D images and the line profile of PS-*b*-PAA LB films transferred at different surface pressures on glass substrates: (a) 8 mN m^{-1}, (b) 30 mN m^{-1}. The spreading solution concentration was 6 mg mL^{-1}.

When transferred at 8 mN m^{-1} and 30 mN m^{-1}, as shown in Fig. 7(a) and (b) respectively, the morphologies of the two films formed from a 6 mg mL^{-1} spreading concentration are significantly different. As exhibited in Fig. 7a, these pictures of films correspond to the pseudoplateau region in the isotherm. The morphology of the light PS aggregate is characterized by a "wormlike" structure. The average height is about 2.4 nm. The darker regions among PS aggregates are supposed to be PAA chains. In this state PAA chains just overlap with each other and parts of PAA chains still absorb at the water surface. After depositing on glass substrates, PAA clusters cannot be fully covered by PS aggregates. The randomly distributed black holes in the topography image are possibly formed after transfer, because dehydration during the drying step causes PAA chains to shrink. At 30 mN m^{-1} surface pressure corresponding to the "brush" region in the isotherm, a continuous "reticular" structure is observed in Fig. 7b. The width of the mesh is less than 83 nm, and the average height is about 4.6 nm. No PAA cluster could be seen in the topography image due to the complete dissolution of PAA chains underneath the PS aggregates. The 3D image shows that surrounded by raised polymer aggregates the meshes formed. The morphologies of meshes are mainly circular, and this is similar to the result in previous research by Joncheray *et al.*[28]

The dramatic morphology change upon surface pressure increase is attributed to the rebuild of PS clusters during lateral compression. In dilute solutions, PS cores formed after dissolution of DMF are loosened, and the PAA chains are at the periphery and bottom of them. It is expected that upon compression the increase in the van der Waals attraction[43] among the PS moieties is accompanied by an increase in the electrostatic and steric repulsion among the PAA chains. As

represented in AFM images, PAA clusters disappear after the surface pressure rises up to 30 mN m^{-1}, which is caused by gradual desorption of PAA chains from the water surface. The aggregates change from relatively dispersive wormlike structures to continuous reticulate structures, implying that the van der Waals attractive force could be larger than the repulsive force among PAA chains. Therefore, the apparent increase in height (from 2.4 to 4.6 nm) has resulted from the "pancake-to-brush" transition of PAA chains and the secondary aggregation of PS clusters.

As shown in Fig. 8a, for a copolymer solution of 9 mg mL^{-1}, AFM images of films deposited at 8 mN m^{-1} represent predominant dot aggregate morphology. The average height of dots is about 2.6 nm. The cloudy darker clusters surrounding light PS dots are supposed to be PAA chains. At 30 mN m^{-1} surface pressure, the morphology is a rugged structure with light dots, darker dimples and black holes, exhibited in Fig. 8b. The height is less than 2.1 nm, slightly lower than that of dots obtained at 8 mN m^{-1}. The formation of these irregular structures is caused by continuous lateral compression of the relatively uncompressible PS cores which are densely packed following the deposition of concentrated copolymer solution on the water surface. These dots are gradually overlapped with each other forming a rugged film.

AFM images of films from a 12 mg mL^{-1} spreading solution transferred at 8 mN m^{-1} and 30 mN m^{-1} are shown in Fig. 9. The topography and 3D images in Fig. 9a exhibit light raised rings surrounded by darker irregular aggregates. The average height of the raised rings is about 1.4 nm. It can be found in 3D images that the height is not identical for single rings while the heights of irregular aggregates between rings are slightly lower. At the surface pressure of 30 mN m^{-1}, the images obtained by AFM show a rough surface of the polymer film with some holes. The average height is about 1.4 nm which is comparable to that

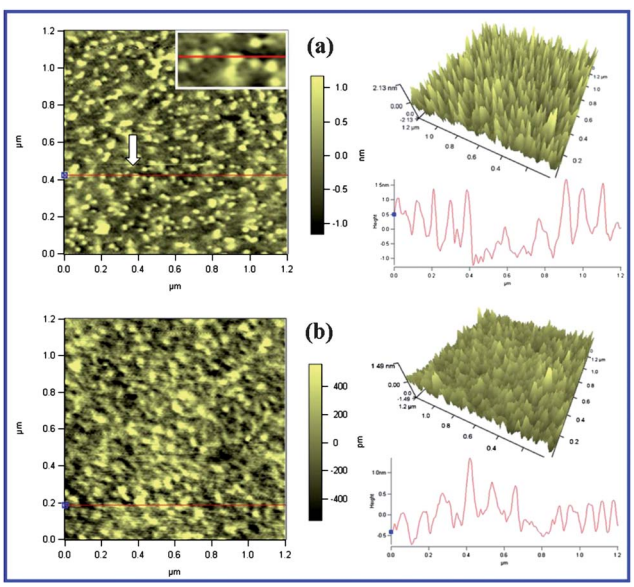

Fig. 8 Topography and 3D images and the line profile of PS-*b*-PAA LB films transferred at different surface pressures on glass substrates: (a) 8 mN m^{-1}, (b) 30 mN m^{-1}. The spreading solution concentration was 9 mg mL^{-1}.

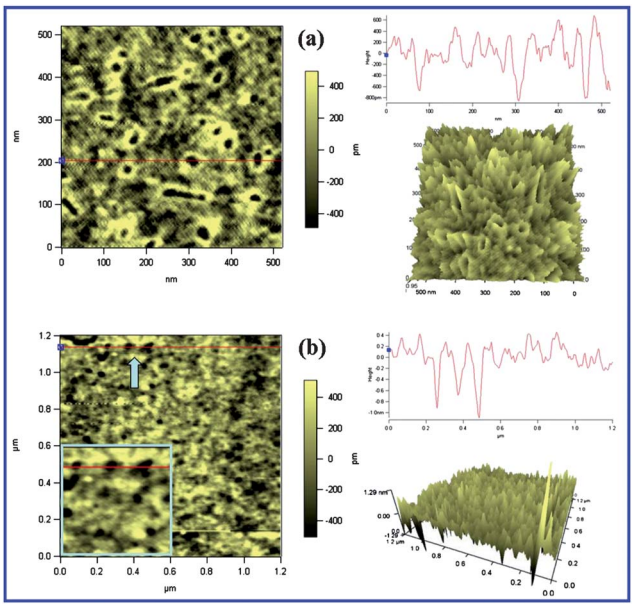

Fig. 9 Topography and 3D images and the line profile of PS-*b*-PAA LB films transferred at different surface pressures on glass substrates: (a) 8 mN m^{-1}, (b) 30 mN m^{-1}. The spreading solution concentration was 12 mg mL^{-1}.

of rings obtained at 8 mN m^{-1}. This kind of transformation of morphologies comes from the compression between neighboring polymer aggregates caused by lateral compression.

From the above results, the changes in polymer aggregate heights obtained from different spreading concentrations and from deposition at different surface pressures are apparent. Different from those more hydrophobic copolymers with longer PS blocks[25,29] where the height changes are mainly attributed to PS aggregates, the PS-*b*-PAA in the present study is more hydrophilic with PAA of wt%~62%. Therefore when deposited on glass substrates the stacking of PAA chains under PS aggregates also plays an important role in the heights of copolymer films obtained. Fig. 10 shows AFM images prepared by firstly lowering and then lifting the glass substrate through the Langmuir film from a 12 mg mL^{-1} spreading solution at 30 mN m^{-1}. The order of layers in the film is PS–PAA–PAA–PS. The result shows that the height of the film is about 5.4 nm which is almost four times that of the single layer film (1.4 nm)

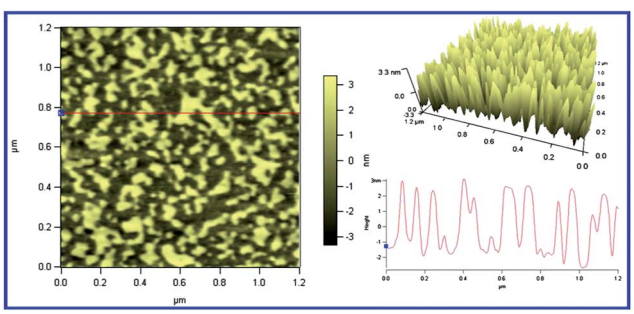

Fig. 10 Topography and 3D images and the line profile of PS–PAA–PAA–PS layers transferred at 30 mN m^{-1}. The spreading solution concentration was 12 mg mL^{-1}.

presented in Fig. 9b. Theoretically it should be two times. The height of the concentrated PS core is relatively stable; thus the change should have resulted from the different arrangement in the PAA–PAA layer and PAA–glass. Furthermore, compared with the single film, it can also be seen that the aggregates are irregular continent-like pieces which is caused by cracking of the film after transfer, as PAA chains at the intermediate layer dehydrate during the drying step. However, we do not have yet at this point more experimental evidence to rationalize this.

Proposed mechanism of two dimensional aggregation formation

From the isotherms, BAM images and the AFM results, we have proposed the mechanism of initial formation of PS-*b*-PAA aggregates at the air–water interface when using DMF as a spreading solvent. The mechanism of copolymer aggregate formation induced by DMF dissolution and affected by the polymer chain dynamics when deposited onto the pure water surface is exhibited in Fig. 11. For a dilute solution, as shown in Fig. 11a, after being deposited onto the water surface, the block copolymers cannot restrict the flow of DMF, and thus its behavior is just like pure DMF. Along with the diffusion of DMF, some holes occur in the film. In this state, the mobility of block copolymer is relatively high, and thus the aggregates are frozen after the diffusion of DMF. The expansion and merging of holes simultaneously result in the break of the continuous copolymer network (shown in Fig. 11a), and thus the irregularly wormlike, loosened morphologies are obtained. For a relatively concentrated solution (Fig. 11b), restricted by the high density and packing of PS chains, the diffusion and flow of solution slow down. Holes in the reticulate structures are polygonal and the block copolymers can gradually flow to the vertexes as shown in Fig. 11b. Therefore after full dissolution of DMF, dot-like aggregates are formed. When the spreading solution is concentrated, as represented in Fig. 11c, the degree of copolymer packing is high enough to restrict the fluidity and let the formation of isolated continent-like aggregates. DMF dissolution only causes formation of some holes in each continent. Meanwhile, attributed to the hole formation and growth, the block copolymers flow to the rims causing raised ring-like aggregates[5,36,37] (models in Fig. 11c). This is also demonstrated by the AFM data (topology and height images in Fig. 8a).

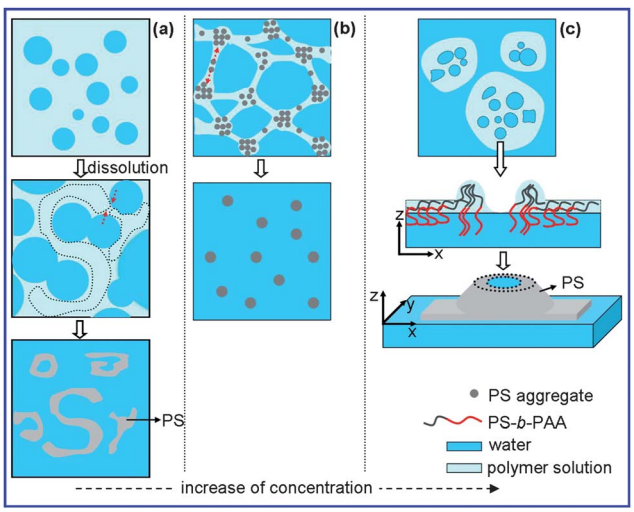

Fig. 11 Mechanism for the initial formation of various PS-*b*-PAA aggregates along with the dissolution of DMF under different spreading solution concentrations. (a) Dilute solution; (b) solution with higher concentration; and (c) concentrated solution.

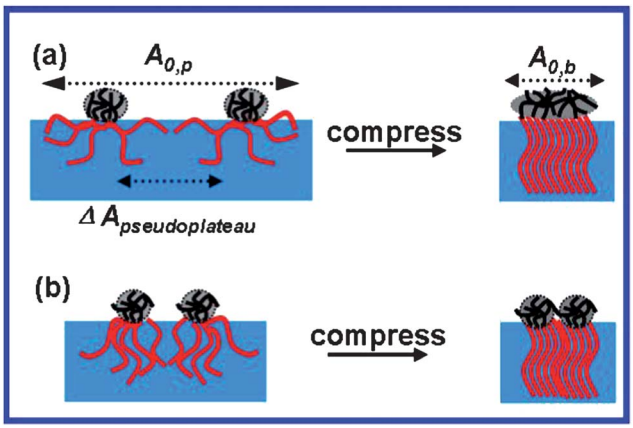

Fig. 12 Qualitative model of copolymer packing and its effect on the pancake-to-brush transition upon compression for PS-*b*-PAA surface aggregates formed from (a) dilute and (b) concentrated spreading solutions, based on concentration-dependent compression isotherm data and AFM images.

The mechanism of conformation transition of the PS-*b*-PAA Langmuir film upon compression can also be deduced. As shown in Fig. 12a, for a dilute solution, the two dimensional aggregates formed after the diffusion of DMF are loosened, and occupy a large surface area. Upon compression, the PAA chains gradually desorb from the interface, and form brush structures underneath the PS cores. Further lateral compression causes an increase in the van der Waals attractive force of PS blocks. The neighboring loosened PS cores combine leading to the aggregates conformation transition. For a concentrated solution (Fig. 12b), the PS cores are densely packed, and thus the steric repulsion between PS and PAA is higher causing the PAA chains to submerge in the water subphase even before compression. Meanwhile, the PS cores are relatively uncompressible, and thus instead of combination, further compression of the film in the brush region could only cause the extrusion of PS clusters, forming a dense film with irregular structures. Therefore the $A_{0,b}$ for films from a concentrated solution include both the surface area of block copolymer and the area of gaps at the joint of aggregates.

Conclusions

In this work, the air–water interfacial self-assembly of more hydrophilic block copolymer PS-*b*-PAA is carried out by using DMF as the co-solvent and pure water as the subphase. The obtained surface pressure–mean molecular area isotherms and AFM images highlight apparent spreading solution concentration and surface pressure dependence of interfacial aggregation

behavior of copolymers. At the same time the hysteresis and relaxation analysis of the copolymer Langmuir film reveal its detailed conformation changes. Furthermore, the LB films prepared have a variety of morphologies such as wormlike, reticulate, porous structures, dots and so on.

According to the isotherms, BAM and AFM images, we draw conclusion that the dissolution of DMF in the water subphase is the initial driving force for the formation of 2D micelles. Meanwhile the different polymer chain dynamics in solutions with different concentrations which have discrepancies in fluidity at the interface are the main reasons for the formation of various films. Moreover, for a dilute spreading solution, in the small mean molecular area region the neighboring PS cores combine with each other upon lateral compression causing the dramatic changes in morphology. However, for a concentrated solution, the polymer aggregates could only compress with each other forming rugged films.

On the basis of these results, we can conclude that by choosing a suitable solvent and controlling the conditions such as spreading solution concentration and surface pressure we can get block copolymer films with target structures. In the future, ultrathin films having special structures, containing block copolymers and other functional materials, could also be prepared through this method.

Acknowledgements

This work is supported by the Key Natural Science Foundation of Shaanxi Province (Grant no. 2009JZ004, 2012JQ1016) and NPU Foundation for Fundamental Research (NPU-FFR-JC20100242, JC201158).

References

1 K. Kita-Tokarczyk, M. Junginger, S. Belegrinou and A. Taubert, *Adv. Polym. Sci.*, 2011, **242**, 151–201.
2 C. A. Devereaux and S. M. Baker, *Macromolecules*, 2002, **35**, 1921–1927.
3 R. B. Cheyne and M. G. Moffitt, *Langmuir*, 2005, **21**, 5453–5460.
4 R. B. Cheyne and M. G. Moffitt, *Langmuir*, 2005, **21**, 10297–10300.
5 R. B. Cheyne and M. G. Moffitt, *Langmuir*, 2006, **22**, 8387–8396.
6 R. B. Cheyne and M. G. Moffitt, *Macromolecules*, 2007, **40**, 2046–2057.
7 E. W. Price, Y. Guo, C. W. Wang and M. G. Moffitt, *Langmuir*, 2009, **25**, 6398–6406.
8 S. Harirchian-Saei, M. C. P. Wang, B. D. Gates and M. G. Moffitt, *Langmuir*, 2010, **26**, 5998–6008.
9 E. W. Price, S. Harirchian-Saei and M. G. Moffitt, *Langmuir*, 2011, **27**, 1364–1372.
10 J. L. Logan, P. Masse, B. Dorvel, A. M. Skolnik, S. S. Sheiko, R. Francis, D. Taton, Y. Gnanou and R. S. Duran, *Langmuir*, 2005, **21**, 3424–3431.
11 J. L. Logan, P. Masse, Y. Gnanou, D. Taton and R. S. Duran, *Langmuir*, 2005, **21**, 7380–7389.
12 S. Peleshanko, J. Jeong, R. Gunawidjaja and V. V. Tsukruk, *Macromolecules*, 2004, **37**, 6511–6522.
13 R. Gunawidjaja, S. Peleshanko and V. V. Tsukruk, *Macromolecules*, 2005, **38**, 8765–8774.
14 R. Francis, D. Taton, J. L. Logan, P. Masse, Y. Gnanou and R. S. Duran, *Macromolecules*, 2003, **36**, 8253–8259.
15 R. Gunawidjaja, S. Peleshanko, K. L. Genson, C. Tsitsilianis and V. V. Tsukruk, *Langmuir*, 2006, **22**, 6168–6176.
16 S. Peleshanko, R. Gunawidjaja, S. Petrash and V. V. Tsukruk, *Macromolecules*, 2006, **39**, 4756–4766.
17 G. Y. Wen, *J. Phys. Chem. B*, 2010, **114**, 3827–3832.
18 I. Perepichka, A. Badia and C. Geraldine Bazuin, *ACS Nano*, 2010, **4**, 6825–6835.
19 P. Kaewsaiha, K. Matsumoto and H. Matsuoka, *Langmuir*, 2007, **23**, 7065–7071.
20 E. Mouri, P. Kaewsaiha, K. Matsumoto, H. Matsuoka and N. Torikai, *Langmuir*, 2004, **20**, 10604–10611.
21 D. H. Xie, C. A. Rezende, G. M. Liu, S. Pispas, G. Z. Zhang and L. T. Lee, *J. Phys. Chem. B*, 2009, **113**, 739–744.
22 H. Matsuoka, Y. Suetomi, P. Kaewsaiha and K. Matsumoto, *Langmuir*, 2009, **25**, 13752–13762.
23 E. Eghbali, O. Colombani, M. Drechsler, A. Müller and H. Hoffmann, *Langmuir*, 2006, **22**, 4766–4776.
24 J. N. Baskir, T. A. Hatton and U. W. Suter, *Macromolecules*, 1988, **21**, 1878–1880.
25 M. Niwa, T. Hayashi and N. Higashi, *Langmuir*, 1990, **6**, 263–268.
26 E. P. K. Currie, A. B. Sieval, M. Avena, H. Zuilhof, E. J. R. Sudhölter and M. A. Cohen Stuart, *Langmuir*, 1999, **15**, 7116–7118.
27 E. P. K. Currie, A. B. Sieval, G. J. Fleer and M. A. Cohen Stuart, *Langmuir*, 2000, **16**, 8324–8333.
28 T. J. Joncheray, S. A. Bernard, R. Matmour, B. Lepoittevin, R. J. El-Khouri, D. Taton, Y. Gnanou and R. S. Duran, *Langmuir*, 2007, **23**, 2531–2538.
29 P. Muller, G. Sudre and O. Théodoly, *Langmuir*, 2008, **24**, 9541–9550.
30 J. K. Cox, K. Yu, B. Constantine, A. Eisenberg and R. Bruce Lennox, *Langmuir*, 1999, **15**, 7714–7718.
31 S. Nagano, Y. Matsushita, Y. Ohnuma, S. Shinma and T. Seki, *Langmuir*, 2006, **22**, 5233–5236.
32 Y. Seo, C. Y. Cho, M. Hwangbo, H. J. Choi and S. M. Hong, *Langmuir*, 2008, **24**, 2381–2386.
33 G. Moad, J. Chiefari, Y. K. Chong, J. Krstina, R. T. A. Mayadunne, A. Postma, E. Rizzardo and S. H. Thang, *Polym. Int.*, 2000, **49**, 993–1001.
34 J. Chiefari, R. T. A. Mayadunne, C. L. Moad, G. Moad, E. Rizzardo, A. Postma, M. A. Skidmore and S. H. Thang, *Macromolecules*, 2003, **36**, 2273–2283.
35 I. Langmuir, *J. Am. Chem. Soc.*, 1916, **39**, 1848–1906.
36 R. A. Segalman and P. F. Green, *Macromolecules*, 1999, **32**, 801–807.
37 G. Lu, W. Li, J. Yao, G. Zhang, B. Yang and J. Shen, *Adv. Mater.*, 2002, **14**, 1049–1053.

38 F. Monroy, H. M. Hilles, F. Ortega and R. G. Rubio, *Phys. Rev. Lett.*, 2003, **91**, 268–302.
39 T. Scopigno, R. D. Leonardo and G. Ruocco, *Phys. Rev. Lett.*, 2004, **92**, 025503.
40 H. Hilles, A. Maestro, F. Monroy, F. Ortega and R. G. Rubio, *J. Phys. Chem.*, 2007, **126**, 124904.
41 D. Y. Zang, E. Rio, D. Langevin, B. Wei and B. P. Binks, *Eur. Phys. J. E: Soft Matter Biol. Phys.*, 2010, **31**, 125–134.
42 D. Y. Zang and Y. J. Zhang, *Sci. China: Earth Sci.*, 2011, **54**, 1587–1592.
43 M. J. Felipe, N. Estillore, R. Pernites, T. Nguyen, R. Ponnapati and R. C. Advincula, *Langmuir*, 2011, **27**, 9327–9336.